Stable Quasi-Solid-State Dye-Sensitized Solar Cells Using Novel Low Molecular Mass Organogelators and Room-Temperature Molten Salts

ARTICLE *in* THE JOURNAL OF PHYSICAL CHEMISTRY C · MARCH 2014

Impact Factor: 4.77 · DOI: 10.1021/jp412717y

THE JOURNAL OF PHYSICAL CHEMISTRY C

Article

pubs.acs.org/JPCC

Stable Quasi-Solid-State Dye-Sensitized Solar Cells Using Novel Low Molecular Mass Organogelators and Room-Temperature Molten Salts

Li Tao,[†,∥] Zhipeng Huo,*[,†,∥] Songyuan Dai,*[,†,‡] Yong Ding,[†] Jun Zhu,[†] Changneng Zhang,[†] Bing Zhang,[‡] Jianxi Yao,[‡] Mohammad K. Nazeeruddin,*[,§] and Michael Grätzel[§]

[†]Key Laboratory of Novel Thin-Film Solar Cells, Division of Solar Energy Materials and Engineering, Institute of Plasma Physics, Chinese Academy of Sciences, Hefei, Anhui, 230031, People's Republic of China

[‡]School of Renewable Energy, North China Electric Power University, No 2, Beinong Rd, Changping, Beijing, 102206, People's Republic of China

[§]Laboratory for Photonics and Interfaces, Institution of Chemical Sciences and Engineering, School of Basic Sciences, Swiss Federal Institute of Technology, CH-1015 Lausanne, Switzerland

Supporting Information

ABSTRACT: Stable quasi-solid-state dye-sensitized solar cells (DSCs) were fabricated by using room-temperature molten salts (1-methyl-3-hexyl-imidazolium iodide), and a series of diamine derivatives with different lengths of alkyl chain as low molecular mass organogelators (LMOGs). The number of methylene ($-CH_2-$) units between the two amide carbonyl groups in the gelator molecule has significant influence on the charge transport property of gel electrolyte, and the kinetic processes of the electron transport and recombination. Less compact networks of the ionic liquid gel electrolytes containing odd-numbered $-CH_2-$ gelator facilitate the diffusion of I_3^- and I^-. Also, the odd-numbered $-CH_2-$ gelators-based DSCs exhibit longer electron recombination lifetime and a higher open circuit potential (V_{oc}) compared with the DSCs based on even-numbered $-CH_2-$ gelators; consequently, the photovoltaic performances of DSCs based on odd-numbered $-CH_2-$ gelators are much better than those even-numbered $-CH_2-$ gelators. Remarkably, the results of the accelerated aging tests showed that the ionic liquid gel electrolyte-based DSCs could retain 93%−99% of their initial photoelectric conversion efficiencies (η) under heat at 60 °C, and 100% of their initial photoelectric conversion efficiencies under one sun light soaking with UV cutoff filter at 50 °C for 1000 h. This excellent long-term stability of quasi-solid-state DSCs is very important for application and commercialization of DSCs.

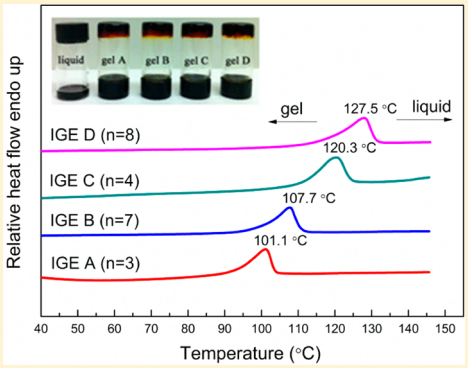

1. INTRODUCTION

The development of clean alternatives to current power generation methods is immensely important to preserve the global environment and ensure sustained economic growth. Photovoltaics offer a clean solution to the energy and environment crisis. Extensive research has been done in the area of dye-sensitized solar cells (DSCs) since the pioneer work of Professor Michael Grätzel and his co-workers on the sensitization of titania, a wide band gap semiconductor with a poly pyridyl ruthenium sensitizer for the fabrication of an efficient and low cost solar cell.[1,2] Although the highest photoelectric conversion efficiency of DSCs based on liquid electrolyte has exceeded 12%,[3] potential problems caused by liquid electrolytes, postures a challenge, and limiting the long-term performance for practical use of DSCs. In order to solve this problem, room-temperature molten salt (ionic liquid) electrolytes (ILEs) for DSCs have been investigated during the past decade because of their unique properties: high ionic conductivity, negligibly low vapor pressure, high thermal and chemical stability, broad electrochemical windows, and non-flammability.[4,5] Also, ionic liquid-based quasi-solid-state electrolytes containing polymer,[6,7] nanoparticles[8−10] or low molecular mass organogelators (LMOGs)[11,12] have been regarded as promising candidates for improving the long-term stability of DSCs.[13−16] To take advantage of the high surface area of the nanoporous TiO_2 film electrode, good contact is of great importance between the dye-anchored electrode and the electrolyte, that is, the electrolyte must fully penetrate into the porous network. LMOGs can finely disperse anisotropic aggregates within the liquid electrolyte, resulting in a three-dimensional structure and effectively make the liquid electrolyte form quasi-solid-state electrolyte with small quantities.[17] At low

Special Issue: Michael Grätzel Festschrift

Received: December 28, 2013
Revised: February 18, 2014
Published: March 7, 2014

dx.doi.org/10.1021/jp412717y | J. Phys. Chem. C 2014, 118, 16718−16726

temperature, LMOGs can self-assemble through H-bonding, van der Waals forces, or $\pi-\pi$ bond staking resulting a network, which immobilizes the solvent molecules, leading to gel formation.[17] Tan et al. reported that bis(4-octanoylaminophenyl) ether, bis(4-octanoylaminophenyl) methane, and 2,4-bis(octanureido) toluene could be used as LMOGs for gelation of ionic liquid, and that the electrochemical properties of the ionic liquid gels were similar to that of the pure ionic liquid.[18] Voss et al. used 12-hydroxysteaic acid to gelate the ionic liquid 1-hexyl-3-methylimidazolium bis-(trifluoromethylsulfonyl)-imide with a small weight percent (1.5 wt %).[12]

In this work, we have synthesized a series of diamine derivatives containing different numbers (3, 7, 4, and 8) of methylene groups ($-CH_2-$) between the two amide carbonyl groups. We used them as LMOGs for quasi-solid-state DSCs based on room-temperature molten salt 1-methyl-3-hexyl-imidazolium iodide (HMII). Subsequently, we systematically studied how the molecular structures of the gelators influence on the electrochemical properties of the gel electrolytes, the photovoltaic performances, and stabilities of the devices. It is interesting that the gel-to-solution transition temperature (T_{gel}) of the gel electrolytes, the electrochemical characteristics, photovoltaic performances, and long-term stabilities of quasi-solid-state DSCs were changed regularly with variation of the even- and odd-numbered $-CH_2-$ in the molecules of the LMOGs. Particularly, the excellent thermal and light-soaking stabilities of quasi-solid-state DSCs assembled with these LMOGs were exhibited during accelerated aging tests.

2. EXPERIMENT

2.1. Synthesis of Four Low Molecular Mass Organogelators. The *N*,*N*′-1,3-propanediylbis-dodecanamide (gelator A); *N*,*N*′-1,7-heptanediylbis-dodecanamide (gelator B), *N*,*N*′-1,4-butanediylbis-dodecanamide (gelator C) and *N*,*N*′-1,8-octanediylbis-dodecanamide (gelator D) were synthesized,[19] and the experimental detailes are shown in the Supporting Information. The gelators were characterized by proton nuclear magnetic resonance spectra (^{1}H NMR) (Bruker Avance III 500, Bruker, Switzerland) and elemental analysis (VarioEL III, Elementar, Germany). Specifically, the gelator A, B, C, and D, each contain three, seven, four, and eight $-CH_2-$ between the two amide carbonyl groups in the molecule structure of gelators (n = 3, 7, 4, and 8), respectively. The structure of these gelator molecules are shown in Figure S1.

2.2. Electrolyte Preparation. HMII was prepared as reported previously.[20] The ionic liquid electrolyte (ILE) for DSC was composed of 0.35 mol L^{-1} iodine (I_2: 99%, Aldrich), 0.02 mol L^{-1} anhydrous lithium iodide (LiI: 99%, Aldrich), and 0.5 mol L^{-1} *N*-methylbenzimidazole (NMBI: 99%, Aldrich) in HMII. Ionic gel electrolytes (IGEs) were prepared by adding 5 wt % (vs ILE) gelators into the ILE, respectively, and heated under stirring until the gelators melted. After cooling to room temperature, IGE A, B, C, and D with gelator A, B, C, and D were formed, respectively.

2.3. Fabrication of Dye-Sensitized Solar Cells. The colloidal TiO_2 microspheres were prepared by hydrolysis of titanium tetraisopropoxide as reported.[21] Nanocrystalline electrodes of 11.3 μm thickness transport layer were obtained by screen-printing TiO_2 paste on FTO glasses (TEC-8, LOF). After sintering at 450 °C for 30 min in air, then cooling to about 120 °C, the nanoporous TiO_2 photoelectrode was immersed in an ethanol solution of 0.5 mM cis-dithiocyanate-*N*,*N*-bis-(4-carboxylate-4-tetrabutylammoniumcarboxylate-2,2-bipyridine) ruthenium(II) (N719 dye) for 14 h. The platinized counter electrodes were obtained by spraying H_2PtCl_6 solution to FTO glass, followed by heating at 410 °C for 20 min. The DSCs were assembled by sealing the dyed nanoporous TiO_2 photoelectrode and the counter electrode with thermal adhesive films (Surlyn 1702, Dupont, USA). The ILE was injected into the internal space between of two electrodes through the holes on the counter electrode, which were later sealed by a cover glass and thermal adhesive film. The IGE was heated to 130 °C under stirring until the gel transform to liquid completely. Then, the electrolyte (hot solution) was rapidly injected into the cell, and the cell was sealed similar to the ILE-based cell. After cooling to room temperature, a uniform motionless gel layer was formed in cell.

2.4. Differential Scanning Calorimetry. The gel-to-solution transition temperature (T_{gel}) of IGE was determined by differential scanning calorimetry (DSC-Q2000, TA, USA). Approximately 5−7 mg of each sample was weighed and sealed in an aluminum pan, and heated at a rate of 10 °C·min^{-1} under nitrogen flow from 25 to 145 °C for DSC measurement.

2.5. Voltammetric Measurements. Steady-state voltammograms were recorded on a electrochemical workstation (Autolab 320, Metrohm, Switzerland) at 25 °C in two-electrode mode of DSC equipped with a 5.0 μm platinum ultramicroelectrode (CHI107, CH InstrumentsInc., USA) as working electrode, a 1 mm radius platinum disk electrode (CHI102, CH InstrumentsInc.,USA) as counter electrode and reference electrode.[22,23] The steady-state current−voltage curves were obtained at a scan rate of 5 mV·s^{-1}.

2.6. Electrochemical Impedance Spectroscopy (EIS) Measurement. EIS measurement of DSCs was recorded with an electrochemical analyzer (Autolab 320, Metrohm, Switzerland). To measure the impedance, a direct-current bias at 600 mV, and a perturbation amplitude of 10 mV within the frequency range from 10 MHz to 10 mHz was applied in the dark. The obtained impedance spectra were fitted with Z-view software (v2.8b, Scribner Associates, USA) in terms of a transmission line equivalent circuit model to interpret the characteristics of DSCs.[24,25]

2.7. Controlled Intensity Modulated Photocurrent/Photovoltage Spectroscopy (IMPS/IMVS) Measurements. The experimental setup for IMPS and IMVS measurements have been described elsewhere.[26−28] Intensity-modulated measurements were carried out by an electrochemical workstation (IM6e, Zahner, Germany) with light emitting diodes (LED) (λ = 610 nm) driven by Export (Zahner, Germany). The LED provided both the dc and ac components of the illumination. A small ac component is 10% or less than that of the dc component, and the frequency range was from 3 kHz to 300 mHz.

2.8. Characterization of Incidental Photon-to-Electron Conversion Efficiency (IPCE). The photocurrent action spectra were recorded on a IPCE measurement kit consisting of a 300 W xenon lamp (69911, Newport, USA), a 1/4 m monochromator (74125 Oriel Cornerstone 260, Newport, USA), a dual channel power meter (2931-C, Newport, USA), and the calibrated UV silicon photodetector (71675, Newport, USA).

2.9. Photovoltaic Characterizations and Stability Tests. The photovoltaic performances of DSCs with the active area of 0.16 cm^2 with black mask were measured by a Keithley 2420 digital source meter (Keithley, USA), and controlled by Test point software under a 450 W xenon lamp (Orial, USA)

dx.doi.org/10.1021/jp412717y | J. Phys. Chem. C 2014, 118, 16718−16726

with a filter (AM 1.5). The incident light intensity was calibrated with a standard crystalline silicon solar cell before test.

Hermetically sealed cells were used for long-term stability tests. The cells were stored in an oven at 60 °C for thermal stress experiment. Furthermore, the data of successive one sun light soaking experiment were also acquired. DSCs covered with a UV cutoff filter (up to 394 nm) were irradiated at open circuit at AM 1.5, (XQ3000, 100 mW·cm^{-2}, Shanghai B.R. Science Instrument Co., Ltd., China), and the ambient temperature was set to 50 °C during the light soaking experiment. $J-V$ measurements were carried out at room temperature after allowing these cells to cool down and equilibrate for 30 min.

3. RESULT AND DISCUSSION

3.1. DSC Characteristics of Electrolytes Containing Different LMOGs. Differential scanning calorimetry is usually used to investigate the gel phase to liquid phase transition of the gel. The transition temperature (T_{gel}) from gel state to liquid state is one of the important parameters to reflect the inherent stability of gel electrolyte responding to external thermo-stimuli. Generally, the high T_{gel} is useful for the application of DSCs to exhibit long-term stability.[29,30] As shown in Figure 1, the T_{gel} values of IGE C (n = 4, 120.3 °C) and IGE D (n = 8, 127.5 °C) are higher than those of IGE A (n = 3, 101.1 °C) and IGE B (n = 7, 107.7 °C). It is interesting that the T_{gel} values of the IGEs-based on the gelators containing even-numbered $-CH_2-$ between the two amide carbonyl groups are higher than those of the IGEs containing odd-numbered $-CH_2-$. This may be attributed to the structural differences in the self-assembly of these gelator molecules, as shown in Figure S2. An even-numbered $-CH_2-$ based diamide molecule forms two pairs of hydrogen bonds with another molecules in a plane, while the odd-numbered $-CH_2-$ based diamide molecule forms four independent hydrogen bonds with four other molecules not in a plane, which leads to the networks of even-numbered $-CH_2-$ based gelators being more compact than those of odd-numbered $-CH_2-$ based gelators.[19,31] Thus, the even-numbered $-CH_2-$ based gel electrolytes (IGE C and IGE D) are more stable than the odd-numbered $-CH_2-$ based gel electrolytes (IGE A and IGE B). On the other hand, comparing the T_{gel} of IGE C with that of IGE D, the T_{gel} value increases with the length of carbon chain, which is due to the increased intermolecular interactions of the alkyl chain by van der Waals force. This phenomenon is also observed in IGE A and IGE B.

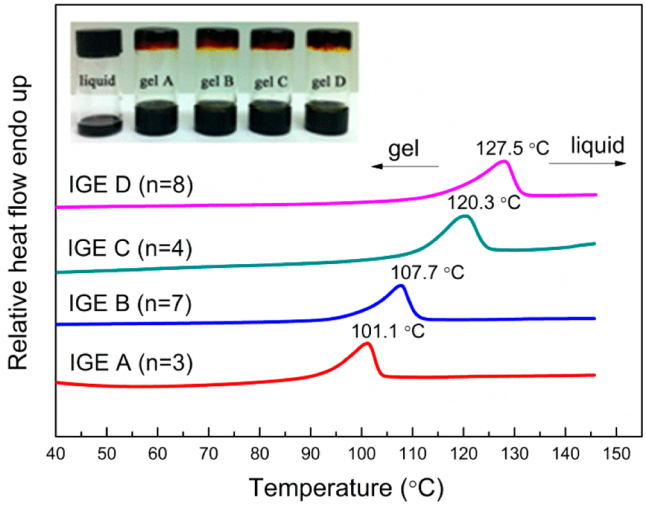

Figure 1. Differential scanning calorimetric thermograms of IGEs with different LMOGs and the photographs of ILE and IGEs.

3.2. The Charge Transport and Electron Recombination Behavior. In DSCs, oxidation of the iodide (I^-) to triiodide (I_3^-) occurs at the photoanode, and this I_3^- must then migrate to the cathode to be reduced, thus there must be sufficient diffusion of the redox species (I^- and I_3^-) through the electrolyte system to compensate for the continuing depletion of the I^- and I_3^- at the photoanode and cathode, respectively.[32] Herein, the ions transport process in the electrolyte was investigated by steady-state voltammograms as shown in Figure 2. The apparent diffusion coefficient (D_{app}) of I^- and I_3^- are calculated from the anodic and cathodic steady−state currents (I_{ss}) using eq 1:[33]

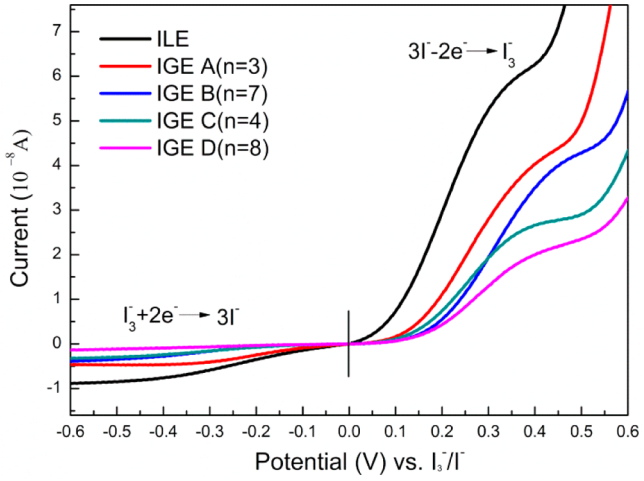

Figure 2. Cyclic voltammograms of HMII-based ILE and IGEs with Pt ultramicroelectrode at 25 °C (scan rate = 5 mV·s^{-1}).

$$I_{ss} = 4nrcFD_{app} \quad (1)$$

where n is the electron number in the electrode reaction, F is the Faraday constant, c is the bulk concentration of electroactive species, and r is the radius of the Pt ultramicroelectrode. As can be seen in Figure 2 and Table 1, when the ILE was gelated by the LMOGs, the D_{app} values of the I^- and I_3^- both decreased. This result indicates that the cross-linked network of the IGE could hinder the physical diffusion of the I^- and I_3^-. Since the networks of IGEs-based on the gelators containing odd-numbered $-CH_2-$ are less obstructive than those of IGEs-based on the gelators containing even-numbered $-CH_2-$ as mentioned above, the redox species are more easily to migrate in IGE A and B than in IGE C and D, which results in the higher D_{app} values of the I^- and I_3^-. The ions transport processes in the IGE A and B are faster than the IGE C and D, which indicates a superior electrochemical activity in IGE A and B compared with that of IGE C and D and leading to much lower power dissipation in DSCs. Moreover, the larger diffusion coefficient of I_3^- plays an important role to increase the short circuit photocurrent density[34] and reduce the dark reaction at the TiO_2 photoelectrode/electrolyte interface in the quasi-solid-state DSCs.[35,36]

dx.doi.org/10.1021/jp412717y | J. Phys. Chem. C 2014, 118, 16718−16726

Table 1. The Steady-State Current and Apparent Diffusion Coefficient of I_3^-/I^- in ILE and IGEs

electrolyte	$I_{ss}(I_3^-)$ (10^{-8} A)	$I_{ss}(I^-)$ (10^{-8} A)	$D_{app}(I_3^-)$ (10^{-7} cm^2·s^{-1})	$D_{app}(I^-)$ (10^{-7} cm^2·s^{-1})
ILE	0.84	6.10	2.18	4.29
IGE A(n = 3)	0.48	3.83	1.24	2.69
IGE B(n = 7)	0.36	3.18	0.93	2.24
IGE C(n = 4)	0.29	2.57	0.75	1.81
IGE D(n = 8)	0.13	1.90	0.34	1.34

To further confirm the improved electron transport in the IGE A and IGE B compared with IGE C and IGE D, we studied the kinetic process at the photoelectrode/electrolyte interfaces of DSCs by EIS. According to Bisquert theory,[37,38] the experimental data were fitted in terms of equivalent circuits, which are depicted in the inset of Figure 3. The interfacial

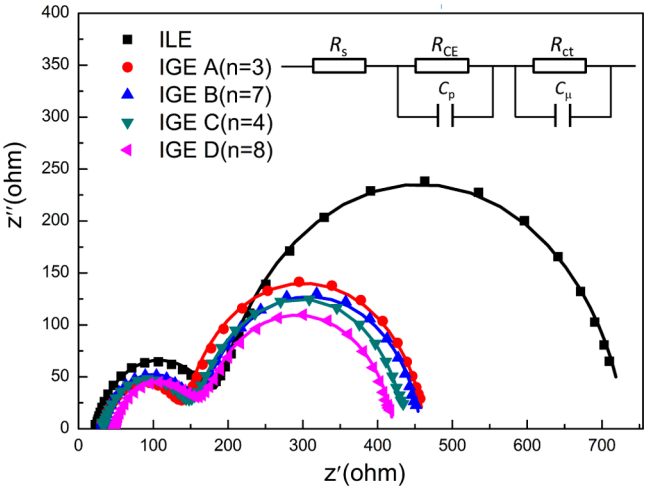

Figure 3. Electrochemical impedance spectroscopy (Nyquist plots) for DSCs based on ILE and IGEs. The lines show the fitted results.

electron recombination resistance and recombination lifetime of the electron in TiO_2 photoanode can be derived from the EIS analysis and list in Table 2.[39,40] Here R_s is the series

Table 2. The Fitting Results of EIS Parameters for the DSCs Based on ILE and IGEs

cell	R_s (Ω)	R_{ct} (Ω)	C_μ (μF)	$\tau_{n(EIS)}$ (s)
ILE	24	547	407	0.22
IGE A(n = 3)	32	321	400	0.13
IGE B(n = 7)	33	296	396	0.12
IGE C(n = 4)	33	287	380	0.11
IGE D(n = 8)	48	255	340	0.09

resistance, R_{ct} is resistance related to electron recombination processes occurring at photoelectrode/electrolyte interfaces, C_μ is the capacitance of this interface, and the obtained recombination lifetime ($\tau_{n(EIS)}$=R_{ct}·C_μ) reflects the electron recombination in the TiO_2 photoelectrode/electrolyte interface. As shown in Table 2, the series resistance of the IGEs-based DSCs increased resulting from the slower charge transport compared with the ILE-based DSC. Generally, the larger the R_{ct} and $\tau_{n(EIS)}$ are, the slighter the electron recombination at the dyed TiO_2 photoelectrode/electrolyte interface is. As can be seen in Table 2, all R_{ct} and $\tau_{n(EIS)}$ of quasi-solid-state DSCs are lower than those of ionic liquid DSC arising from the slower diffusion of I_3^- and the capture of conduction band electrons in nanoporous TiO_2 photoelectrode by I_3^- ions. Nevertheless, the R_{ct} and $\tau_{n(EIS)}$ of quasi-solid-state DSCs based on the IGE A and IGE B are obviously higher than those of quasi-solid-state DSCs based on the IGE C and IGE D. It is indicated that charge recombination is suppressed in DSCs based on the IGE A and IGE B compared with the DSCs based on the IGE C and IGE D owing to the faster charge transport.

As is known, the chemical capacitance C_μ corresponds to trap energy distribution below the conduction band edge and is directly related to the energy difference between ${}_nE_F$−$E_{F,redox}$ in accordance with eq 2:[41,42]

$$C_\mu = C_0 \exp\left(\alpha \frac{({}_nE_F - E_{F,redox})}{k_B T}\right) \quad (2)$$

where ${}_nE_F$ is the quasi-Fermi level that determines the electron occupation of the trap and conduction band states, $E_{F,redox}$ is the energy difference between the quasi-Fermi level and the redox Fermi level, C_0 is the prefactor of the exponential, k_B is Boltzmann constant, $\alpha = T/T_0$, T_0 is the characteristic temperature of distribution, and T is the temperature.[43] The lower C_μ value indicates a higher upward displacement of the TiO_2 conduction band edge. In this case, we can speculate that the TiO_2 conduction band edges of cells based on IGE C and IGE D are more negative than those of cells based on IGE A and IGE B, which results from the lower C_μ.

3.3. Shift of TiO_2 Conduction Band Edge. It is known that the small-radius Li^+ in electrolyte can intercalate into the mesoporous dye-coated nanocrystalline TiO_2 film and form an ambipolar Li^+−e^- with the electron in the conduction band of TiO_2, which increases the transport rate of electrons in nanocrystalline TiO_2, and enhances electron injection efficiency from an excited state of the dye due to the positive shift of TiO_2 conduction band edge.[44−47] On the other hand, Li^+ can interact with the amide carbonyl groups of the gelator molecule in the gel electrolyte.[48] Therefore, the different self-assembly behaviors of the four gelators have different effects on the adsorption of Li^+ on the surface of the mesoporous TiO_2 film and further influence the kinetic processes of the gel electrolyte-based DSCs.

The photoinduced charge (Q) in the mesoporous TiO_2 films was detected by IMPS/IMVS measurements. The dependence of V_{oc} on ln Q is shown in Figure 4. The TiO_2 conduction band edge shift can be analyzed by comparing the change of V_{oc} at a given Q, and the relationship between V_{oc} and ln(Q) derived from a linear eq 3:

$$V_{oc} = V_c + m_c \ln(Q) \quad (3)$$

where m_c is the slope rate and V_c is the vertical intercept.[49] According to the difference in V_c, the TiO_2 conduction band edges of quasi-solid-state DSCs based on IGE A, IGE B, IGE C, and IGE D shift negatively 18, 20, 22, and 39 mV, respectively, in comparing with ILE-based DSCs. This phenomenon is attributed to the decreased adsorption of Li^+ on the TiO_2

dx.doi.org/10.1021/jp412717y | J. Phys. Chem. C 2014, 118, 16718−16726

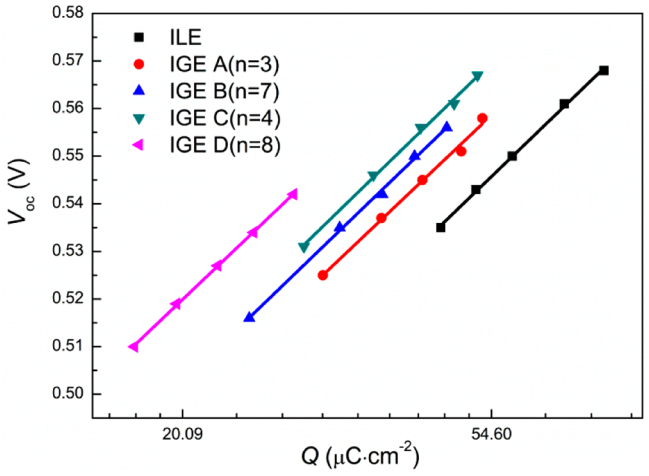

Figure 4. Voltage dependence of the photoinduced electrondensity in the DSCs based on ILE and IGEs.

surface owing to the interaction between Li^+ and the amide carbonyl groups of the LMOGs. Moreover, because the networks of IGEs-based on gelators containing even-numbered $-CH_2-$are more compact than those containing odd-numbered $-CH_2-$,[19,31] the IGE C and IGE D exhibit stronger steric hindrance effects on the Li^+ adsorption on the TiO_2 surface than the IGE A and IGE B. Consequently, the TiO_2 conduction band edges of IGE C- and IGE D-based DSCs shift to more negative potential than those IGE A- and IGE B-based DSCs. In addition, the steric hindrance effect is increased with the increase of the alkyl chain length of the gelators; as a result, the TiO_2 conduction band edge of the IGE D-based DSC (n = 8) shifts to more negative potential than that of the IGE C-based DSC (n = 4). This result can also be obtained between IGE B- and IGE A-based DSCs (n = 7, and 3). Based on the analysis above, we can speculate that the electron injection efficiency (φ_{inj}) was in the order of ILE > IGE A> IGE B > IGE C > IGE D for these DSCs, and the higher φ_{inj} makes a contribution to the higher IPCE.

3.4. Photovoltaic Performance of Quasi-Solid-State DSCs. Improving the efficiencies of quasi-solid-state DSCs will ultimately require optimization of electron transport time (τ_d) and electron recombination lifetime (τ_n), which can be obtained from IMPS and IMVS studies, respectively.[50] Figure 5a,b displays light intensity dependencies on τ_d and τ_n in the DSCs based on ILE and IGEs. It is accepted that as the Li^+ density in the films increases, the τ_d and τ_n of photoelectrons increase proportionately.[45,51] The IGEs-based DSCs have much shorter τ_d and τ_n than those of the ILE-based DSC, which results from the decreased Li^+ absorption on the surface of TiO_2 films in IGEs-based DSCs. On the other hand, the amount of absorption of Li^+ on the surface of TiO_2 films in DSCs based on IGE A and IGE B are more than those in DSCs based on IGE C and IGE D, resulting in longer τ_d and τ_n. As can be seen in Figure 5b, the recombination between conduction band electrons and I_3^- was suppressed in IGE A- and IGE B-based DSCs when compared with the IGE C- and IGE D-based DSCs, which is consistent with the results by EIS study. Figure 6 shows the dark current−voltage characteristics

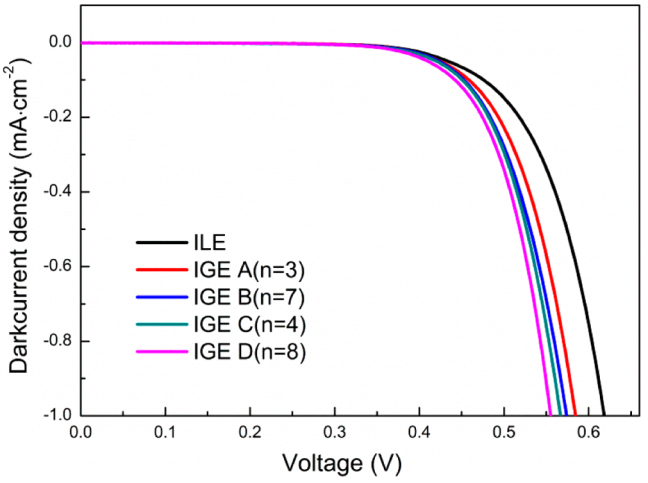

Figure 6. J−V curves of the DSCs based on ILE and IGEs in dark conditions.

of the ILE- and IGEs-based DSCs. As can be seen, the dark currents of IGEs-based DSCs are larger than that of ILE-based DSC, which results from the slower transport of I_3^- ions from the dyed TiO_2/electrolyte interface to the counter electrode. Thus, the electron recombination at the interface between the nanoporous TiO_2 photoelectrode and the electrolyte increases in the IGEs-based DSCs. On the other hand, the dark currents of IGE A- and IGE B-based DSCs are lower than those of IGE C- and IGE D-based DSCs, which is caused by the less compact

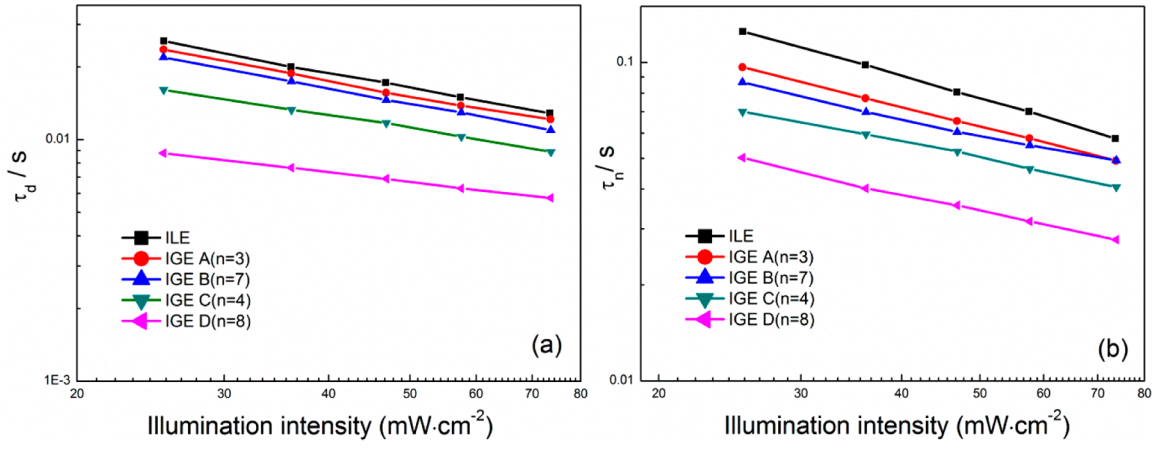

Figure 5. Light intensity dependence of electron transport times (τ_d) and recombination lifetimes (τ_n) in DSCs based on ILE and IGEs.

dx.doi.org/10.1021/jp412717y | J. Phys. Chem. C 2014, 118, 16718−16726

networks of IGE A and IGE B providing a less obstructed channel for charge diffusion than the IGE C and IGE D.

Figure 7 shows a typical photocurrent density−voltage curve at AM 1.5 and IPCE spectra for DSCs based on ILE and IGEs.

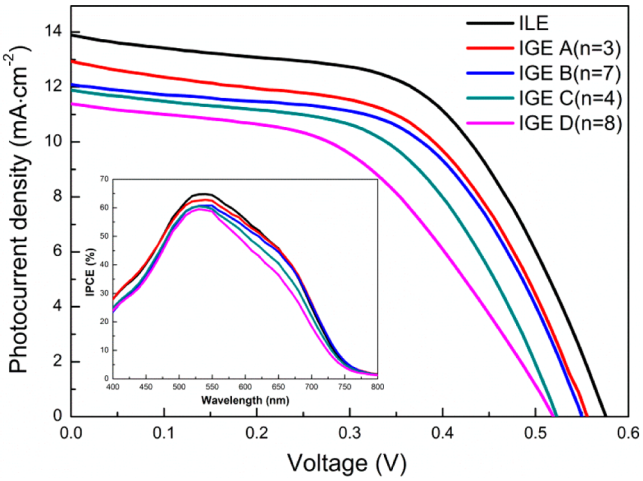

Figure 7. IPCE spectra and $J-V$ curves of the DSCs based on ILE and IGEs at AM 1.5.

The photovoltaic performances of open circuit potential (V_{oc}), short circuit photocurrent density (J_{sc}), fill factor (FF), and photoelectric conversion efficiency (η) are listed in Table 3. It

Table 3. Photovoltaic Performance Parameters of DSCs Based on ILE and IGEs at AM 1.5

cell	V_{oc} (mV)	J_{sc} (mA·cm^{-2})	FF	η (%)
ILE	575	13.95	0.56	4.46
IGE A(n = 3)	554	13.00	0.55	3.92
IGE B(n = 7)	549	12.16	0.56	3.78
IGE C(n = 4)	522	11.94	0.54	3.41
IGE D(n = 8)	518	11.44	0.49	2.91

is widely considered that the TiO_2 conduction band edge position and electron recombination are two essential factors affecting the V_{oc}. After ILE was gelated by LMOGs, a negative shift in TiO_2 conduction band edge indicates a contribution to the increased V_{oc}[49] (as is shown in Scheme 1). However, as can be seen in Table 3, all V_{oc} values of quasi-solid-state DSCs are lower than that of ionic liquid-based DSCs, which can definitely be attributed to the increased recombination in quasi-solid-state DSCs due to the slower diffusion of redox species in the gel networks. This result is well confirmed with the lower R_{ct}, recombination lifetime and D_{app} of I_3^- for the IGEs-based DSCs in comparison with the ILE-based DSC. Moreover, compared with the IGE C- and IGE D-based DSCs, the recombination at the TiO_2 photoelectrode/electrolyte interface were decreased in the IGE A- and IGE B-based DSCs due to the much faster diffusion of I_3^- resulting from the less obstructive networks of the odd-numbered $-CH_2-$ based IGEs. As a result, the V_{oc} of the IGE A- and IGE B-based DSCs are higher than those of the IGE C- and D-based DSCs. In addition, IGE A- and IGE B-based DSCs exhibit higher J_{sc} due to both the faster diffusion of I_3^- and the higher IPCE of the corresponding devices.[34] Consequently, the photoelectric conversion efficiencies of the DSCs based on IGE A and IGE B are much better than those of the DSCs based on IGE C and IGE D, which can be comparable with the ILE-based device.

3.5. Stability of Quasi-Solid-State DSCs Fabricated Using LMOGs. Although the photovoltaic performances of these four types of quasi-solid-state DSCs based on LMOGs are lower than the corresponding ILE-based DSC, they exhibit excellent long-term stability. As is shown in Figure 8, the photoelectric conversion efficiency of the ILE-based DSC retained 83% of the initial value, however, all the quasi-solid-state DSCs retained 93%−99% after 60 °C thermal stress for 1000 h. Remarkably, during successive one sun light soaking for 1000 h, with an UV filter, all IGEs-based DSCs maintained the original photoelectric conversion efficiency, while the ILE-based DSC retained only 85% of its initial value. These accelerated aging results reveal that the networks of the IGEs-based DSCs are more stable than the ILE-based DSC, which is caused by the good intrinsic stability of the LMOGs and the high T_{gel} of the IGEs.

4. CONCLUSION

In conclusion, a series of diamine derivatives containing different numbers of $-CH_2-$ groups (n = 3, 7, 4, 8) between the two amide carbonyl groups in the molecular structure were synthesized and successfully developed as LMOGs to gelate the HMII-based ILE. The T_{gel} values of these ionic gel electrolytes are all above 100 °C, which is an advantage to the long-term stability of quasi-solid-state DSCs. The differences of molecular structures between odd- and even-numbered $-CH_2-$ based gelators can lead to a different network of gel electrolyte, which results in significant influences on the charge diffusion, electron recombination, TiO_2 conduction band edge shift and photovoltaic performances of quasi-solid-state DSCs. Compared with the IGEs-based on the gelators containing even-numbered $-CH_2-$, the less compact networks of the IGEs-based on the odd-numbered $-CH_2-$ gelators can facilitate the transport of redox species (I^- and I_3^-) and contribute to the higher J_{sc}. Moreover, the fast diffusion of I^- and I_3^- can suppress the electron recombination reaction at the TiO_2/electrolyte interface, which results in the longer recombination lifetime

Scheme 1. Shift of TiO_2 Conduction Band Edge after the ILE Was Gelated by LMOGs

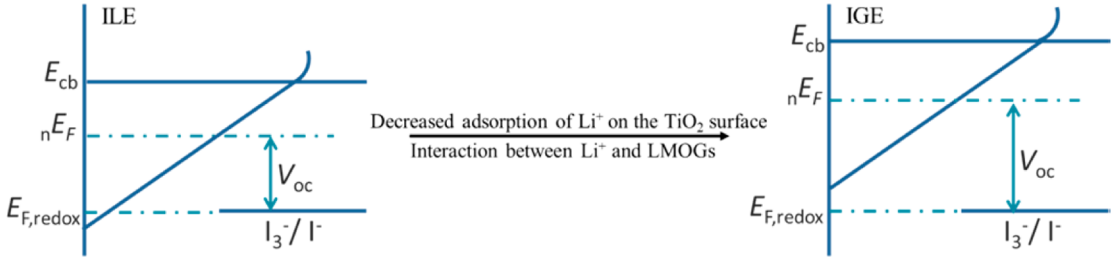

dx.doi.org/10.1021/jp412717y | J. Phys. Chem. C 2014, 118, 16718−16726

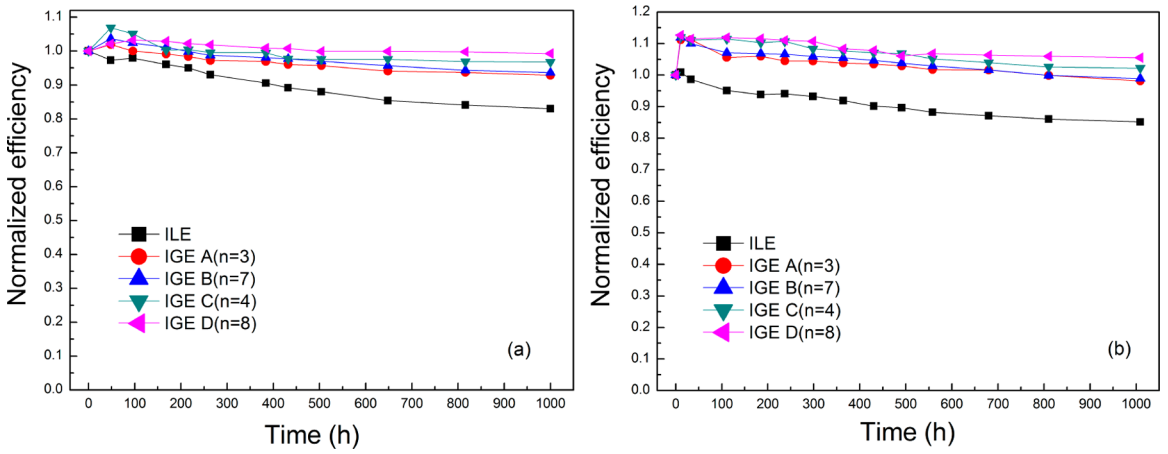

Figure 8. (a) Normalized efficiency variation with the DSCs based on ILE and IGEs at 60 °C for 1000 h and (b) successive one sun light soaking with UV cutoff filter at 50 °C for 1000 h.

and contributes to the improved V_{oc}. Consequently, the photoelectric conversion efficiency of cells based on the gelators containing odd-numbered $-CH_2-$ are higher than those DSCs based on the gelators containing even-numbered $-CH_2-$ and can be comparable with the ILE-based DSC. More importantly, the accelerated aging tests show that the gelation led to excellent durability of the devices almost without losing their photovoltaic performances, which is important for application and commercialization of DSCs.

■ ASSOCIATED CONTENT

Supporting Information

Detailed chemical structures, synthesis procedures, ^{1}H NMR spectra and results of Elements analysis of gelators. This information is available free of charge via the Internet at http://pubs.acs.org.

■ AUTHOR INFORMATION

Corresponding Authors

*E-mail: zhipenghuo@163.com; Phone: +86 551 65592190 (Z.P.H.).

*E-mail: sydai@ipp.ac.cn; Phone: +86 10 61772268 (S.Y.D.).

*E-mail: mdkhaja.nazeeruddin@epfl.ch; Phone: +41 21 69 36124 (M.K.N.).

Author Contributions

‖L.T. and Z.P.H. contributed equally to this work.

Notes

The authors declare no competing financial interest.

■ ACKNOWLEDGMENTS

This work was supported by the National Basic Research Program of China (No. 2011CBA00700), Sino Swiss Science and Technology Cooperation Program (No. IZLCZ2_139056), External cooperation program of Chinese Academy of Science (No. GJHZ1220), the National High Technology Research and Development Program of China (No. 2011AA050510), the National Natural Science Foundation of China (No. 21103197 and 21173227), and the Program of Hefei Center for Physical Science and Technology (No. 2012FXZY006).

■ REFERENCES

(1) O'Regan, B.; Grätzel, M. A. Low-Cost, High-Efficiency Solar-Cell Based on Dye-Sensitized Colloidal TiO_2 Films. *Nature* **1991**, *353*, 737−740.

(2) Grätzel, M. Cluster Physics - All Surface and No Bulk. *Nature* **1991**, *349*, 740−741.

(3) Yella, A.; Lee, H. W.; Tsao, H. N.; Yi, C. Y.; Chandiran, A. K.; Nazeeruddin, M. K.; Diau, E. W. G.; Yeh, C. Y.; Zakeeruddin, S. M.; Gratzel, M. Porphyrin-Sensitized Solar Cells with Cobalt (II/III)-Based Redox Electrolyte Exceed 12% Efficiency. *Science* **2011**, *334*, 629−634.

(4) Sun, S.; Song, J.; Feng, R.; Shan, Z. Ionic Liquid Gel Electrolytes for Quasi-Solid-State Dye-Sensitized Solar Cells. *Electrochim. Acta* **2012**, *69*, 51−55.

(5) Ogawa, H.; Unemoto, A.; Honma, I. Quasi-Solid-State Lithium-Sulfur Battery Using Room Temperature Ionic Liquid-Li-Salt-Fumed Silica Nanoparticle Composites as Electrolytes. *Electrochemistry* **2012**, *80*, 765−767.

(6) Chang, L. Y.; Lee, C. P.; Vittal, R.; Lin, J. J.; Ho, K. C. Enhanced Performance of a Dye-Sensitized Solar Cell with an Amphiphilic Polymer-Gelled Ionic Liquid Electrolyte. *J. Mater. Chem. A* **2013**, *1*, 3055−3060.

(7) Yu, Z.; Qin, D.; Zhang, Y.; Sun, H.; Luo, Y.; Meng, Q.; Li, D. Quasi-Solid-State Dye-Sensitized Solar Cell Fabricated with Poly(*β*-Hydroxyethyl Methacrylate) Based Organogel Electrolyte. *Energy Environ. Sci.* **2011**, *4*, 1298−1305.

(8) Chi, W. S.; Roh, D. K.; Kim, S. J.; Heo, S. Y.; Kim, J. H. Hybrid Electrolytes Prepared from Ionic Liquid-Grafted Alumina for High-Efficiency Quasi-Solid-State Dye-Sensitized Solar Cells. *Nanoscale* **2013**, *5*, 5341−5348.

(9) Huang, S.; Wang, X.; Wong, C. C. Silica Nanoparticle Gelled Ionic Electrolyte for Dye Sensitized Solar Cells. *Nanosci. Nanotechnol. Lett.* **2013**, *5*, 542−545.

(10) Lee, H. F.; Wu, J. L.; Hsu, P. Y.; Tung, Y. L.; Ouyang, F. Y.; Kai, J. J. Enhanced Photovoltaic Performance and Long-Term Stability of Dye-Sensitized Solar Cells by Incorporating SiO_2 Nanoparticles in Binary Ionic Liquid Electrolytes. *Thin Solid Films* **2013**, *529*, 2−6.

(11) Tu, T.; Bao, X.; Assenmacher, W.; Peterlik, H.; Daniels, J.; Doetz, K. H. Efficient Air-Stable Organometallic Low-Molecular-Mass Gelators for Ionic Liquids: Synthesis, Aggregation and Application of Pyridine-Bridged Bis(benzimidazolylidene)-Palladium Complexes. *Chem.—Eur. J.* **2009**, *15*, 1853−1861.

(12) Voss, B. A.; Bara, J. E.; Gin, D. L.; Noble, R. D. Physically Gelled Ionic Liquids: Solid Membrane Materials with Liquidlike CO_2 Gas Transport. *Chem. Mater.* **2009**, *21*, 3027−3029.

(13) Tan, S. X.; Zhai, J.; Xue, B. F.; Wan, M. X.; Meng, Q. B.; Li, Y. L.; Jiang, L.; Zhu, D. B. Property Influence of Polyanilines on

Photovoltaic Behaviors of Dye-Sensitized Solar Cells. *Langmuir* **2004**, *20*, 2934−2937.
(14) Mohan, V. M.; Murakami, K.; Kono, A.; Shimomura, M. Poly(acrylonitrile)/Activated Carbon Composite Polymer Gel Electrolyte for High Efficiency Dye Sensitized Solar Cells. *J. Mater. Chem. A* **2013**, *1*, 7399−7407.
(15) Li, Y.; Lee, D. K.; Kim, J. Y.; Kim, B.; Park, N. G.; Kim, K.; Shin, J. H.; Choi, I. S.; Ko, M. J. Highly Durable and Flexible Dye-Sensitized Solar Cells Fabricated on Plastic Substrates: PVDF-Nanofiber-Reinforced TiO_2 Photoelectrodes. *Energy Environ. Sci.* **2012**, *5*, 8950−8957.
(16) Dissanayake, M. A. K. L.; Thotawatthage, C. A.; Senadeera, G. K. R.; Bandara, T. M. W. J.; Jayasundara, W. J. M. J. S. R.; Mellander, B. E. Efficiency Enhancement in Dye Sensitized Solar Cells Based on PAN Gel Electrolyte with Pr_4NI + MgI_2 Binary Iodide Salt Mixture. *J. Appl. Electrochem.* **2013**, *43*, 891−901.
(17) Terech, P.; Weiss, R. G. Low Molecular Mass Gelators of Organic Liquids and the Properties of Their Gels. *Chem. Rev.* **1997**, *97*, 3133−3159.
(18) Tan, L.; Dong, X.; Wang, H.; Yang, Y. Gels of Ionic Liquid C(4)mim PF6 Formed by Self-Assembly of Gelators and Their Electrochemical Properties. *Electrochem. Commun.* **2009**, *11*, 933−936.
(19) Tomioka, K.; Sumiyoshi, T.; Narui, S.; Nagaoka, Y.; Iida, A.; Miwa, Y.; Taga, T.; Nakano, M.; Handa, T. Molecular Assembly and Gelating Behavior of Didodecanoylamides of α,ω-Alkylidenediamines. *J. Am. Chem. Soc.* **2001**, *123*, 11817−11818.
(20) Shi, C.; Ge, Q.; Han, S.; Cai, M.; Dai, S.; Fang, X.; Pan, X. An Improved Preparation of 1-Methyl-3-Propylimidazolium Iodide and Its Application in Dye-Sensitized Solar Cells. *Solar Energy* **2008**, *82*, 385−388.
(21) Huang, F.; Chen, D.; Zhang, X. L.; Caruso, R. A.; Cheng, Y. B. Dual-Function Scattering Layer of Submicrometer-Sized Mesoporous TiO_2 Beads for High-Efficiency Dye-Sensitized Solar Cells. *Adv. Funct. Mater.* **2010**, *20*, 1301−1305.
(22) Zhang, C.; Dai, J.; Huo, Z.; Pan, X.; Hu, L.; Kong, F.; Huang, Y.; Sui, Y.; Fang, X.; Wang, K.; Dai, S. Influence of 1-Methylbenzimidazole Interactions with Li^+ and TiO_2 on the Performance of Dye-Sensitized Solar Cells. *Electrochim. Acta* **2008**, *53*, 5503−5508.
(23) Lovelock, K. R. J.; Cowling, F. N.; Taylor, A. W.; Licence, P.; Walsh, D. A. Effect of Viscosity on Steady-State Voltammetry and Scanning Electrochemical Microscopy in Room Temperature Ionic Liquids. *J. Phys. Chem. B* **2010**, *114*, 4442−4450.
(24) Bisquert, J. Theory of the Impedance of Electron Diffusion and Recombination in a Thin Layer. *J. Phys. Chem. B* **2002**, *106*, 325−333.
(25) Adachi, M.; Sakamoto, M.; Jiu, J.; Ogata, Y.; Isoda, S. Determination of Parameters of Electron Transport in Dye-Sensitized Solar Cells Using Electrochemical Impedance Spectroscopy. *J. Phys. Chem. B* **2006**, *110*, 13872−13880.
(26) Peter, L. M.; Wijayantha, K. G. U. Electron Transport and Back Reaction in Dye Sensitised Nanocrystalline Photovoltaic Cells. *Electrochim. Acta* **2000**, *45* (28), 4543−4551.
(27) Fisher, A. C.; Peter, L. M.; Ponomarev, E. A.; Walker, A. B.; Wijayantha, K. G. U. Intensity Dependence of the Back Reaction and Transport of Electrons in Dye-Sensitized Nanacrystalline TiO_2 Solar Cells. *J. Phys. Chem. B* **2000**, *104*, 949−958.
(28) Dloczik, L.; Ileperuma, O.; Lauermann, I.; Peter, L. M.; Ponomarev, E. A.; Redmond, G.; Shaw, N. J.; Uhlendorf, I. Dynamic Response of Dye-Sensitized Nanocrystalline Solar Cells: Characterization by Intensity-Modulated Photocurrent Spectroscopy. *J. Phys. Chem. B* **1997**, *101*, 10281−10289.
(29) Mohmeyer, N.; Kuang, D. B.; Wang, P.; Schmidt, H. W.; Zakeeruddin, S. M.; Grätzel, M. An Efficient Organogelator for Ionic Liquids to Prepare Stable Quasi-Solid-State Dye-Sensitized Solar Cells. *J. Mater. Chem.* **2006**, *16*, 2978−2983.
(30) Mohmeyer, N.; Wang, P.; Schmidt, H. W.; Zakeeruddin, S. M.; Grätzel, M. Quasi-Solid-State Dye Sensitized Solar Cells with 1,3:2,4-Di-*O*-Benzylidene-D-Sorbitol Derivatives as Low Molecular Weight Organic Gelators. *J. Mater. Chem.* **2004**, *14*, 1905−1909.
(31) Sumiyoshi, T.; Nishimura, K.; Nakano, M.; Handa, T.; Miwa, Y.; Tomioka, K. Molecular Assembly of C-2-Symmetric Bis-(2s)-2-Methyldodecanoylamides of α,ω-Alkylidenediamines into Coiled Coil and Twisted Ribbon Aggregates. *J. Am. Chem. Soc.* **2003**, *125*, 12137−12412.
(32) Pringle, J. M.; Armel, V. The Influence of Ionic Liquid and Plastic Crystal Electrolytes on the Photovoltaic Characteristics of Dye-Sensitised Solar Cells. *Int. Rev. Phys. Chem.* **2011**, *30*, 371−407.
(33) Wang, P.; Zakeeruddin, S. M.; Comte, P.; Exnar, I.; Gratzel, M. Gelation of Ionic Liquid-Based Electrolytes with Silica Nanoparticles for Quasi-Solid-State Dye-Sensitized Solar Cells. *J. Am. Chem. Soc.* **2003**, *125*, 1166−1167.
(34) Asano, T.; Kubo, T.; Nishikitani, Y. Electrochemical Properties of Dye-Sensitized Solar Cells Fabricated with PVDF-Type Polymeric Solid Electrolytes. *J. Photochem. Photobiol. A* **2004**, *164*, 111−115.
(35) Huo, Z. P.; Dai, S. Y.; Zhang, C. G.; Kong, F. T.; Fang, X. Q.; Guo, L.; Liu, W. Q.; Hu, L. H.; Pan, X.; Wang, K. J. Cells. Low Molecular Mass Organogelator Based Gel Electrolyte with Effective Charge Transport Property for Long-Term Stable Quasi-Solid-State Dye-Sensitized Solar Cells. *J. Phys. Chem. B* **2008**, *112*, 12927−12933.
(36) Huo, Z. P.; Zhang, C. N.; Fang, X. Q.; Cai, M. L.; Dai, S. Y.; Wang, K. J. Low Molecular Mass Organogelator Based Gel Electrolyte Gelated by a Quaternary Ammonium Halide Salt for Quasi-Solid-State Dye-Sensitized Solar Cells. *J. Power Sources* **2010**, *195*, 4384−4390.
(37) Fabregat-Santiago, F.; Garcia-Belmonte, G.; Mora-Sero, I.; Bisquert, J. Characterization of Nanostructured Hybrid and Organic Solar Cells by Impedance Spectroscopy. *Phys. Chem. Chem. Phys.* **2011**, *13*, 9083−9118.
(38) Yan, K.; Chen, W.; Yang, S. Significantly Enhanced Open Circuit Voltage and Fill Factor of Quantum Dot Sensitized Solar Cells by Linker Seeding Chemical Bath Deposition. *J. Phys. Chem. C* **2013**, *117*, 92−99.
(39) Subramanian, A.; Wang, H. W. Effect of Hydroxyl Group Attachment on TiO_2 Films for Dye-Sensitized Solar Cells. *Appl. Surf. Sci.* **2012**, *258*, 7833−7838.
(40) Tang, X.; Wang, Y.; Cao, G. Effect of the Adsorbed Concentration of Dye on Charge Recombination in Dye-Sensitized Solar Cells. *J. Electroanal. Chem.* **2013**, *694*, 6−11.
(41) Fabregat-Santiago, F.; Mora-Sero, I.; Garcia-Belmonte, G.; Bisquert, J. Cyclic Voltammetry Studies of Nanoporous Semiconductors. Capacitive and Reactive Properties of Nanocrystalline TiO_2 Electrodes in Aqueous Electrolyte. *J. Phys. Chem. B* **2003**, *107*, 758−768.
(42) Guillen, E.; Peter, L. M.; Anta, J. A. Electron Transport and Recombination in Zno-Based Dye-Sensitized Solar Cells. *J. Phys. Chem. C* **2011**, *115*, 22622−22632.
(43) Bisquert, J. Chemical Capacitance of Nanostructured Semiconductors: Its Origin and Significance for Nanocomposite Solar Cells. *Phys. Chem. Chem. Phys.* **2003**, *5*, 5360−5364.
(44) Koops, S. E.; O'Regan, B. C.; Barnes, P. R. F.; Durrant, J. R. Parameters Influencing the Efficiency of Electron Injection in Dye-Sensitized Solar Cells. *J. Am. Chem. Soc.* **2009**, *131*, 4808−4818.
(45) Kopidakis, N.; Benkstein, K. D.; van de Lagemaat, J.; Frank, A. J. Transport-Limited Recombination of Photocarriers in Dye-Sensitized Nanocrystalline TiO_2 Solar Cells. *J. Phys. Chem. B* **2003**, *107*, 11307−11315.
(46) Kopidakis, N.; Neale, N. R.; Frank, A. J. Effect of an Adsorbent on Recombination and Band-Edge Movement in Dye-Sensitized TiO_2 Solar Cells: Evidence for Surface Passivation. *J. Phys. Chem. B* **2006**, *110*, 12485−12489.
(47) Pelet, S.; Moser, J. E.; Gratzel, M. Cooperative Effect of Adsorbed Cations and Iodide on the Interception of Back Electron Transfer in the Dye Sensitization of Nanocrystalline TiO_2. *J. Phys. Chem. B* **2000**, *104*, 1791−1795.
(48) Liu, J.; Xia, X.; Li, Y.; Wang, H.; Li, Z. Theoretical Study on the Interaction of Glutathione with Group IA (Li^+, Na^+, K^+), IIA (Be^{2+}, Mg^{2+}, Ca^{2+}), and IIIA (Al^{3+}) Metal Cations. *Struct. Chem.* **2013**, *24*, 251−261.

(49) Ren, X.; Feng, Q.; Zhou, G.; Huang, C. H.; Wang, Z. S. Effect of Cations in Coadsorbate on Charge Recombination and Conduction Band Edge Movement in Dye-Sensitized Solar Cells. *J. Phys. Chem. C* **2010**, *114*, 7190−7195.
(50) Chen, H. Y.; Lin, L.; Yu, X. Y.; Qiu, K. Q.; Lu, X. Y.; Kuang, D. B.; Su, C. Y. Dextran Based Highly Conductive Hydrogel Polysulfide Electrolyte for Efficient Quasi-Solid-State Quantum Dot-Sensitized Solar Cells. *Electrochim. Acta* **2013**, *92*, 117−123.
(51) Watson, D. F.; Meyer, G. J. Cation Effects in Nanocrystalline Solar Cells. *Coord. Chem. Rev.* **2004**, *248*, 1391−1406.